Electronic Supplementary Material (ESI) for Dalton Transactions.

Macrocyclic {3d-4f} SMMs as building blocks for 1D-polymers: selective bridging of 4f ions by use of an O-donor ligand

Sébastien Dhers,[a] Humphrey L. C. Feltham,[a] Mathieu Rouzières,[b,c] Rodolphe Clérac[b,c]* and Sally Brooker[a]*

[a] Department of Chemistry and the MacDiarmid Institute for Advanced Materials and Nanotechnology, University of Otago, PO Box 56, Dunedin 9054, New Zealand. Fax: +64-3-479 7906; Tel: +64-3-479 7919; e-mail: sbrooker@chemistry.otago.ac.nz.

[b] CNRS, CRPP, UPR 8641, F-33600 Pessac, France; Fax: (+33) 5 56 84 56 00; Tel: (+33) 5 56 84 56 50; e-mail: clerac@crpp-bordeaux.cnrs.fr.

[c] Univ. Bordeaux, CRPP, UPR 8641, F-33600 Pessac, France

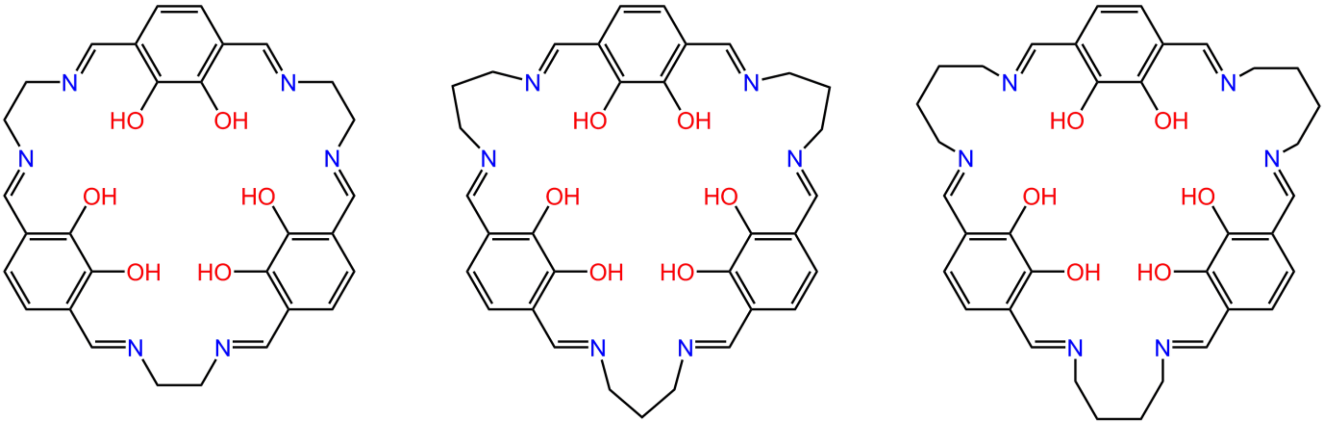

H_6L^{Et} H_6L^{Pr} H_6L^{Bu}

Figure S1. The three macrocycles referred to in this paper, $H_6\mathbf{L}^{\mathbf{R}}$. All three are derived from a metal templated 3+3 Schiff base condensation of 1,4-diformyl-2,3-dihydroxybenzene with the appropriate diamine, either 1,2-diaminoethane ($H_6\mathbf{L}^{\mathbf{Et}}$; ethylene linker), 1,3-diaminopropane ($H_6\mathbf{L}^{\mathbf{Pr}}$; propylene linker) or 1,4-diaminobutane ($H_6\mathbf{L}^{\mathbf{Bu}}$; butylene linker), and are obtained as metal complexes (not metal free). The systematic names are: $H_6\mathbf{L}^{\mathbf{Et}}$ = 3,6,13,16,23,26-hexaazatetracyclo[26.2.2.$2^{8,11}$.$2^{18,21}$]-hexatriaconta-2,6,8,9,10,12,16,18,19,20,26,28,29,30,31-pentadecaene-9,10,19,20,29,30-hexol, $H_6\mathbf{L}^{\mathbf{Pr}}$ = 3,7,14,18,25,29-hexaazatetracyclo[29.2.2.$2^{9,12}$.$2^{20,23}$]-nonatriaconta-2,7,9,10,11,13,18,20,21,22,24,29,31,33,34-pentadecaene-10,11,21,22,32,33-hexol, $H_6\mathbf{L}^{\mathbf{Bu}}$ = 3,8,15,20,27,32-hexaazatetracyclo[32.2.2.$2^{10,13}$.$2^{22,25}$]dotetraconta-2,8,10,12,14,20,22,24,26,32,34,36,37,39,-41-pentadecaene-11,12,23,24,35,36-hexol.

Experimental section

Disodium terephthalate[1] ($Na_2[tpa]$) and 1,4-diformyl-2,3-dihydroxybenzene[2] were synthesised as described in the literature. The solvents used were reagent grade and were used as received from commercial suppliers. All reactions were conducted in air.

IR spectra were recorded as solids on a Bruker Alpha FT-ATR IR spectrometer with a diamond anvil Alpha-P module between 400 and 4000 cm^{-1}. Standard microanalysis was carried out by the Campbell Microanalytical Laboratory at the University of Otago.

X-ray crystallography. Data were collected on an Oxford Diffraction SuperNova diffractometer equipped with a Cryostream N_2 open-flow cooling device at 100 K, using graphite monochromated Cu-Kα radiation. Scans were performed in such a way as to collect a complete set of unique reflections to a maximum resolution of 0.80 Å. Raw frame data (including data reduction, inter-frame scaling, unit cell refinement and absorption corrections) for all structures were processed using *CrysAlis Pro*.[3] Structures were solved using *SUPERFLIP*[4] and refined against all F^2 data using *SHELXL-97*.[5] Hydrogen atoms on carbon atoms were inserted at calculated positions and rode on the atoms to which they were attached, with U(H) = 1.2 × (U)C. Hydrogen atoms on oxygen atoms were inserted at calculated positions that optimised hydrogen bonding and fixed. Details specific to each structure follow:

Single crystals of building block **1**: $[Cu^{II}_3Tb(\mathbf{L^{Et}})(NO_3)_3(MeOH)]\cdot MeOH$. One reflection was OMITed due to its low hkl (001) and discrepancy between found and calculated intensities ($Fo^2 = 1$; $Fc^2 = 543$), indicating it was behind the beamstop. All non-hydrogen atoms were refined with anisotropic thermal ellipsoid parameters. No disorder was observed.

Single crystals of chain polymer **2**: $\{[Cu^{II}_3Tb^{III}(\mathbf{L^{Et}})(tpa)(H_2O)_3](NO_3)\cdot 0.5H_2O\cdot 0.25MeOH\}_n$. The non-coordinated solvent content consists of one half-occupancy water and one a quarter-occupancy methanol over the same site. Bond distances in the methanol molecule and also in the non-coordinated nitrate anion were restrained with DFIX to give reasonable values. For the non-coordinated nitrate anion, a FLAT command was used to keep it planar and an ISOR command to give reasonable thermal ellipsoid parameters. The non-hydrogen atoms of the quarter occupancy methanol molecule were refined isotropically.

Crystallographic data have been deposited with the Cambridge Crystallographic Data Centre (CCDC 1502822 and 1502823).

Magnetic properties. The magnetic susceptibility measurements were obtained with the use of MPMS-XL Quantum Design SQUID magnetometer and PPMS-9 susceptometer. These magnetometer and susceptometer work between 1.8 and 400 K for dc applied fields ranging from -7 to 7 T (MPMS-XL; at around 80 – 400 $Oe.min^{-1}$ for $H < 1$ T and 500 – 2500 $Oe.min^{-1}$ for $H > 1$ T). Measurements were performed on air dried analytically pure polycrystalline samples (12.77 and 14.76 mg for **1**, 12.68 mg for **2**, 16.30 and

11.09 mg for **3**, and 37.880 and 13.040 for **4**) introduced in a polyethylene bag (3 × 0.5 × 0.02 cm, typically 15 to 35 mg) and covered by mineral oil (typical 3 to 8 mg) to avoid torquing effects. ac susceptibility measurements were measured with an oscillating ac field of 1 to 6 Oe with frequency between 10 to 10000 Hz (PPMS). The magnetic data were corrected for the sample holder, mineral oil and the diamagnetic contribution.

Synthesis of $[Cu^{II}_3Tb^{III}(L^{Et})(NO_3)_3(H_2O)]\cdot5H_2O$ (1)

To a solution of 1,4-diformyl-2,3-dihydroxybenzene (0.05 g, 0.3 mmol) in MeOH (5 mL) was added $Cu^{II}(OAc)_2\cdot H_2O$ (0.06 g, 0.3 mmol) suspended in a solution of $Tb^{III}(NO_3)_3.5H_2O$ (0.09 g, 0.2 mmol) in MeOH (10 mL), resulting in a dark brown solution. After stirring the reaction for two hours and being careful to check that all the $Cu^{II}(OAc)_2\cdot H_2O$ had dissolved, 1,2-diaminoethane (1.5 mL of a 0.2 $molL^{-1}$ MeOH solution, 0.3 mmol) was added dropwise, resulting in a yellow-brown solution. The reaction was stirred for a further ten minutes before Et_2O was vapour diffused into the solution. The resulting solid was filtered and dried briefly in air to remove the Et_2O before being dissolved in MeOH : DMF (9:1, 4 mL) and Et_2O vapour diffused into the solution. The resulting solid was filtered and washed with Et_2O (2 × 5 mL) and air giving $[Cu^{II}_3Tb^{III}(\mathbf{L}^{Et})(NO_3)_3(H_2O)]\cdot5H_2O$ as brown powder (0.03 g, 41%). Found: C, 29.99; H, 3.09; N, 10.34. Calculated for $C_{30}H_{36}N_9O_{21}Cu_3Tb$: C, 29.82; H, 3.00; N, 10.43. IR (FT-ATR diamond anvil) $\overline{n}$ / cm^{-1} = 1625 (m); 1516 (w); 1450 (m); 1315 (s); 1237 (m); 1174 (m); 1076 (w); 1039 (m); 970 (w); 937 (w); 829 (m); 784 (w); 730 (m); 662 (w); 643 (m); 624 (w); 600 (m); 570 (w); 522 (w); 456 (m).

Synthesis of $\{[Cu^{II}_3Tb^{III}(L^{Et})(tpa)(H_2O)_3](NO_3)\cdot3.5H_2O\cdot2MeOH\}_n$ (2)

A colourless solution of $Na_2[tpa]$ (26.6 mg, 123.8 μmol) in H_2O/MeOH (1:1, 100 mL) was layered on top of a brown solution of **1** (53.0 mg, 44.1 μmol) in H_2O/MeOH (2:1, 100 mL) in 10 different sample tubes. Dark red crystals of **2** formed after a few weeks. These were filtered off, washed with diethyl ether and air dried (15.2 mg, 35%). Found: C, 37.77; H, 3.10; N, 7.41%. Calculated for $C_{40}H_{43}N_7O_{18.5}Cu_3Tb$ ($\{[Cu^{II}_3Tb^{III}(\mathbf{L}^{Et})(tpa)(H_2O)_3](NO_3)\cdot3.5H_2O\cdot2MeOH\}_n$): C, 37.91; H, 3.42; N, 7.74%. IR (FT-ATR diamond anvil) $\overline{n}$ / cm^{-1} = 3362 (b), 1625 (s), 1587 (m), 1548 (m), 1512 (m), 1448 (s), 1315 (s), 1236 (s), 1171 (m), 1077 (w), 1043 (w),1012 (w), 936 (w), 884 (w), 844 (w), 827 (m), 729 (m), 615 (m), 622 (w), 597 (s), 570 (m), 516 (m), 497 (m), 453 (s).

Synthesis of $Zn^{II}_3Tb^{III}(L^{Et})(NO_3)_2OAc\cdot4H_2O\cdot MeOH$ (3)

To a solution of 1,4-diformyl-2,3-dihydroxybenzene (0.1 g, 0.6 mmol) in MeOH (5 mL) was added a solution of $Zn^{II}(OAc)_2\cdot2H_2O$ (0.132 g, 0.6 mmol) and $Ln^{III}(NO_3)_3\cdot xH_2O$ (0.2 mmol) in MeOH (10 mL), resulting in an orange solution. After stirring the solution overnight, 1,2-diaminoethane (3 mL of 0.2 $molL^{-1}$ MeOH solution, 0.18 mmol) was added dropwise. This reaction was stirred for a further five minutes before being left the stand for three days. The resulting precipitate was filtered, washed with cold MeOH (2 × 5 mL) and dried in air giving $Zn^{II}_3Tb^{III}(\mathbf{L}^{Et})(NO_3)_2OAc\cdot4H_2O\cdot MeOH$ (1206.78 $gmol^{-1}$) as orange powder (0.225 g, 93%). Found: C, 32.72; H, 2.91; N, 8.89; 16.0; Tb, 13.6. Calculated for $Zn^{II}_3Tb^{III}C_{33}H_{39}N_8O_{19}$: C, 32.84; H, 3.26; N, 9.29; Zn, 16.3; Tb, 13.2. Orange powder (0.225 g, 93%). IR (FT-ATR diamond anvil) $\overline{n}$ / cm^{-1} = 1625 (s); 1579 (m); 1510 (w); 1462 (m); 1446 (s); 1396 (m); 1332 (m); 1314 (w); 1235 (m); 1217 (w); 1165 (m); 1124 (w); 1085 (m); 1029 (br); 986 (w); 924 (m); 826 (m); 774 (m); 716 (m); 631 (m); 600 (m); 590 (m); 504 (m); 426 (m).

Synthesis of $\mathbf{Cu^{II}_3La^{III}(L^{Et})(NO_3)_3\cdot MeOH\cdot 3H_2O\cdot DMF}$ (4)

Synthesised in an analogous fashion to **1**, using 0.1 g of 1,4-diformyl-2,3-dihydroxybenzene, giving $Cu^{II}_3La^{III}(\mathbf{L^{Et}})(NO_3)_3\cdot MeOH\cdot 3H_2O\cdot DMF$ (1239.30 $gmol^{-1}$) as brown powder (0.172 g, 62%). Found: C, 32.92; H, 2.92; N, 11.13; Cu, 14.4; La, 11.0. Calculated for $Cu^{II}_3La^{III}C_{34}H_{41}N_{10}O_{20}$: C, 32.95; H, 3.33; N, 11.30; Cu, 15.4; La, 11.2. IR (FT-ATR diamond anvil) $\overline{n}$ / cm^{-1} = 1622 (m); 1514 (w); 1448 (m); 1314 (s); 1236 (m); 1170 (m); 1081 (w); 1040 (m); 978 (w); 939 (w); 828 (m); 784 (w); 732 (m); 668 (w); 642 (m); 621 (w); 601 (m); 572 (w); 519 (w); 456 (m).

Table S1. Structural refinement details for **1** and **2**.

	1	**2**
Empirical formula	$C_{32}H_{32}N_9O_{17}Cu_3Tb$	$C_{153}H_{144}N_{28}O_{67}Tb_4Cu_{12}$
Formula weight	1164.21	4845.12
Temperature (K)	92(2)	100(2)
Wavelength (Å)	0.71073	1.54184
Crystal system	Triclinic	Monoclinic
Space group	P-1	$P2_1/c$
a (Å)	10.3774(12)	13.28540(10)
b (Å)	10.9073(13)	22.9612(2)
c (Å)	17.1427(19)	13.53520(10)
α (°)	91.742(5)	90
β (°)	93.680(5)	95.6920(10)
γ (°)	106.816(5)	90
Volume (Å^3)	1851.1(4)	4108.54(6)
Z	2	1
Calculated density (Mg/m^3)	2.089	1.958
Absorption coefficient (mm^{-1})	3.680	10.795
F(000)	1150	2402
Crystal size (mm^3)	0.21 × 0.10 × 0.04	0.20 × 0.15 × 0.05
Theta range for data collection (°)	4.78 to 52.9	3.34 to 76.75
Index ranges	$-12 \leq h \leq 12$, $-13 \leq k \leq 13$, $-21 \leq l \leq 21$	$-16 \leq h \leq 16$, $-28 \leq k \leq 28$, $-16 \leq l \leq 14$
Reflections collected	21504	42932
Independent reflections	7413 [*R*(int) = 0.0436]	8565 [*R*(int) = 0.0476]
Completeness to theta = 26.45° (%)	97.0	98.9
Absorption correction	Semi-empirical from equivalents	Semi-empirical from equivalents
Max. and min. transmission	0.8668 and 0.5121	0.6144 and 0.2214
Refinement method	Full-matrix least-squares on F^2	Full-matrix least-squares on F^2
Data / restraints / parameters	7413 / 0 / 559	8565 / 28 / 604
Goodness-of-fit on F^2	1.142	1.151
Final *R* indices [$I > 2\sigma(I)$]	$R_1 = 0.0518$, $wR_2 = 0.1173$	$R_1 = 0.0594$, $wR_2 = 0.1898$
R indices (all data)	$R_1 = 0.0601$, $wR_2 = 0.1218$	$R_1 = 0.0676$, $wR_2 = 0.1927$
Largest diff. peak and hole (e.Å^{-3})	1.862 and -1.207	1.680 and -1.380

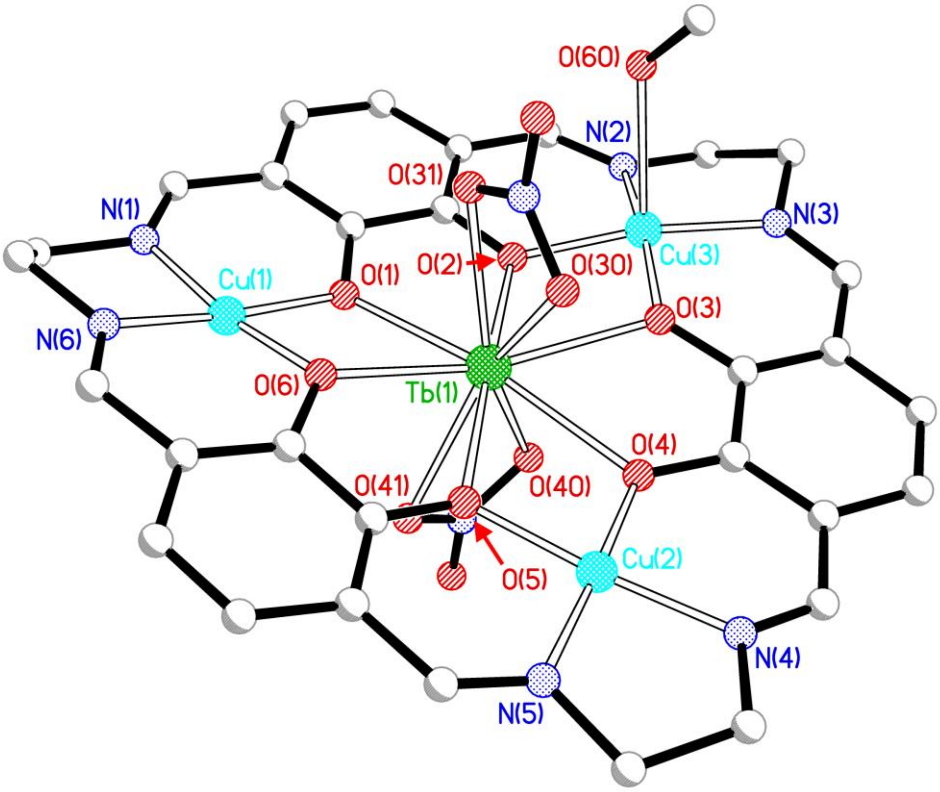

Figure S2. Perspective view of the crystal structure of the SMM building block, $[\mathrm{Cu}^{\mathrm{II}}_3\mathrm{Tb}^{\mathrm{III}}(\mathbf{L}^{\mathbf{Et}})(\mathrm{NO}_3)_3(\mathrm{MeOH})]\cdot\mathrm{MeOH}$ (**1**), with the numbering of all non-H atoms shown. The non-coordinated methanol molecule and hydrogen atoms have been omitted for clarity. Carbon, nitrogen, oxygen, copper and terbium atoms are represented in grey, blue, red, cyan and green, respectively.

Table S2. Comparison of selected bond lengths (Å) and M-M' distances (Å) for the building block **1** and the cationic 1D coordination polymer **2** (M-M' separations quoted are the shortest).

X - range (*average*)	**1**	**2**
Cu geometries	square pyramidal/square planar [a]	square pyramidal
τ(Cu)	0.02 – 0.03 (*0.025*)	0.02 – 0.09 (*0.053*)
Cu-N_{imine}	1.915 – 1.939 (*1.926*)	1.902 – 1.954 (*1.929*)
Cu-O_{cat}	1.886 – 1.909 (*1.896*)	1.886 – 1.912 (*1.894*)
Cu-O_{axial} [b]	2.390 and 2.468 (*2.429*)	2.364 – 2.377 (*2.373*)
Tb geometry (coord. n°)	tetradecahedron (10)	hula-hoop (9)
Tb-O_{cat}	2.432 – 2.507 (*2.472*)	2.462 – 2.489 (*2.476*)
Tb-O_{axial}	2.455 – 2.515 (*2.485*)	2.260 – 2.563 (*2.410*)
Cu···Cu (intra)	6.211	6.114
Cu···Tb (intra)	3.515	3.556
Cu···Cu (intrachain)	-	6.962
Cu···Cu (intermolecular)	6.336	6.084
Tb···Tb (intrachain)	-	11.514
Tb···Tb (intermolecular)	9.559	9.783

[a] only one Cu is square planar. [b] O_{axial}: nitrate in **1** and terephthalate in **2**

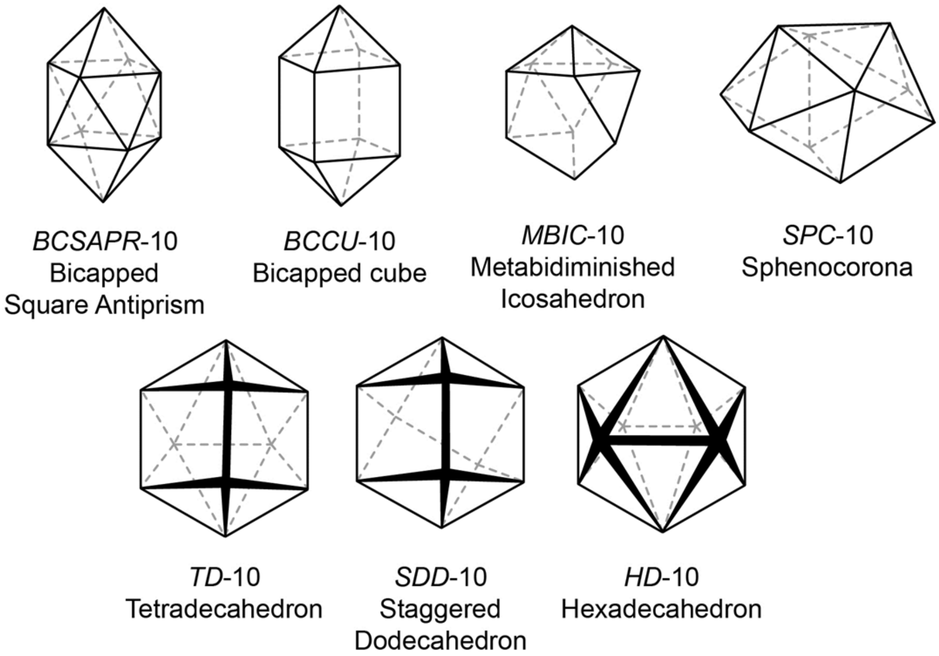

Figure S3. Different geometries for polyhedra with ten vertices.[6]

Table S3. Results of the SHAPE[7] analysis for the Tb^{III} ion for **1**. These idealised ten coordinate geometries are shown in Figure S3. If the value of the SHAPE analysis is 0 then the corresponding structure is fully coincident in shape with the reference polyhedron P, whereas the maximum allowed value of 100 corresponds to the hypothetical case in which all atoms of the molecule occupy the same point in space.

geometry of Tb^{III}	JBCCU-10[b]	JBCSAPR-10[b]	JMBIC-10[b]	JSPC-10[b]	SDD-10[b]	TD-10[b]	HD-10[b]
in **1**	8.696	5.375	6.129	3.843	1.823	**1.416**	5.366

[b] JBCCU-10 (Elongated square bipyramid J15): bicapped cube, *D4h*; JBCSAPR-10 (Gyroelongated square bipyramid J17): bicapped square antiprism, *D4d*; JMBIC-10 (J62): Metabidiminished icosahedron, *C2v*; JSPC-10 (J87): Sphenocorona, *C2v*; SDD-10: Staggered dodecahedron (2:6:2)#, *D2*; TD-10: Tetradecahedron (2:6:2), *C2v*; HD-10: Hexadecahedron (2:6:2, or 1:4:4:1), *D4h*.

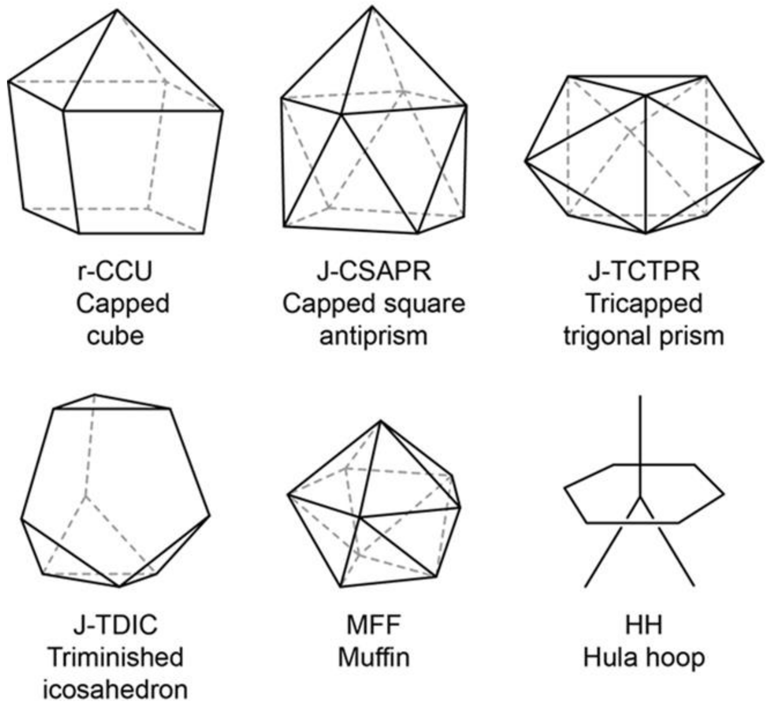

Figure S4. Different geometries for polyhedra with nine vertices.[8]

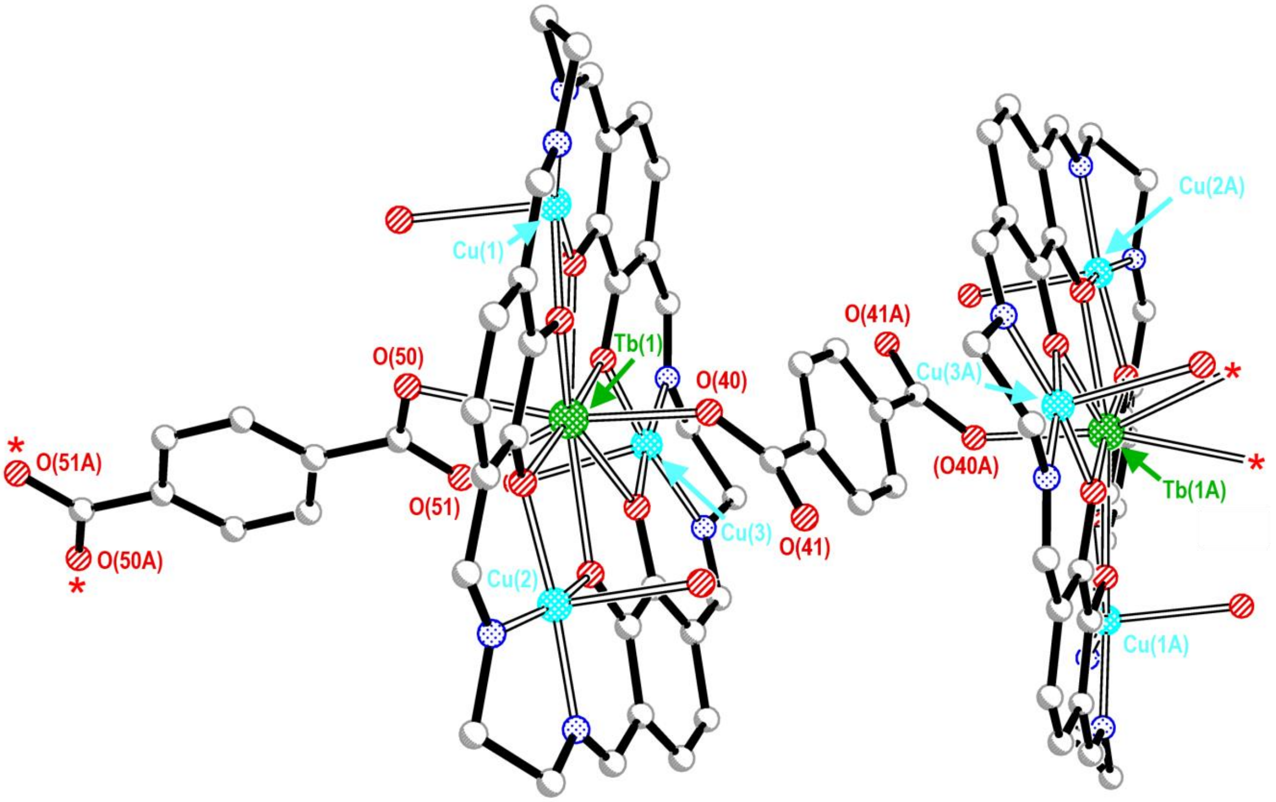

Figure S5. Perspective view of the crystal structure of the chain complex $\{[Cu^{II}_3Tb^{III}(\mathbf{L^{Et}})(tpa)(H_2O)_3](NO_3)\cdot0.5H_2O\cdot0.25MeOH\}_n$ (**2**), showing a numbered close-up view of the repeating units of the structure. The non-coordinated methanol and water molecules, the non-coordinated nitrate anion and hydrogen atoms have been omitted for clarity. The asterisks indicate where the polymer continues. Carbon, nitrogen, oxygen, copper and terbium atoms are represented in grey, blue, red, cyan and green, respectively.

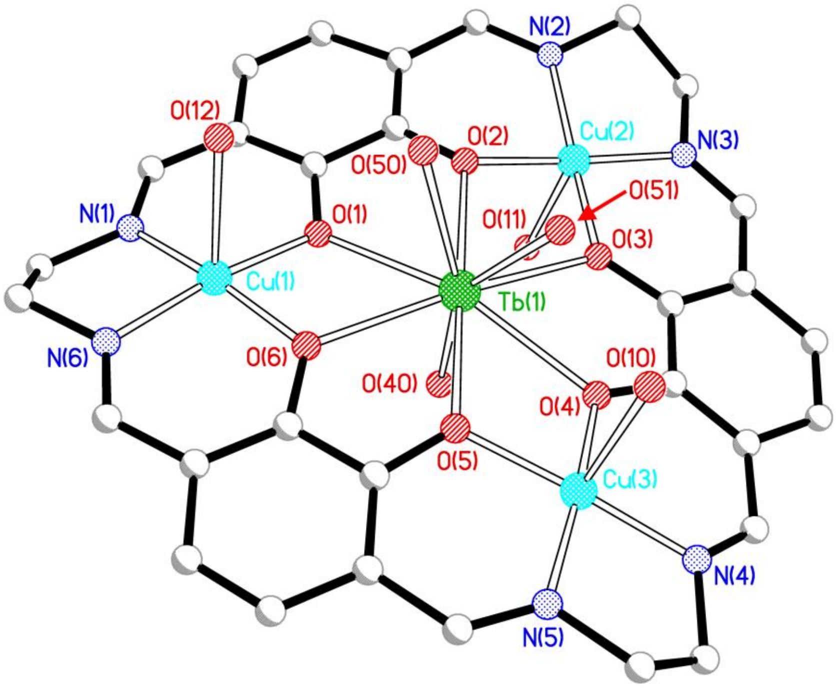

Figure S6. Perspective view of the part of the crystal structure of the chain complex $\{[\mathrm{Cu}^{\mathrm{II}}{}_3\mathrm{Tb}^{\mathrm{III}}(\mathbf{L}^{\mathbf{Et}})(\mathrm{tpa})(\mathrm{H_2O})_3](\mathrm{NO_3})\cdot0.5\mathrm{H_2O}\cdot0.25\mathrm{MeOH}\}_n$ (**2**), showing the unique macrocycle in the asymmetric unit, with all non-H atoms numbered. The non-coordinated methanol and water molecules, the non-coordinated nitrate anion and hydrogen atoms have been omitted for clarity. Carbon, nitrogen, oxygen, copper and terbium atoms are represented in grey, blue, red, cyan and green, respectively.

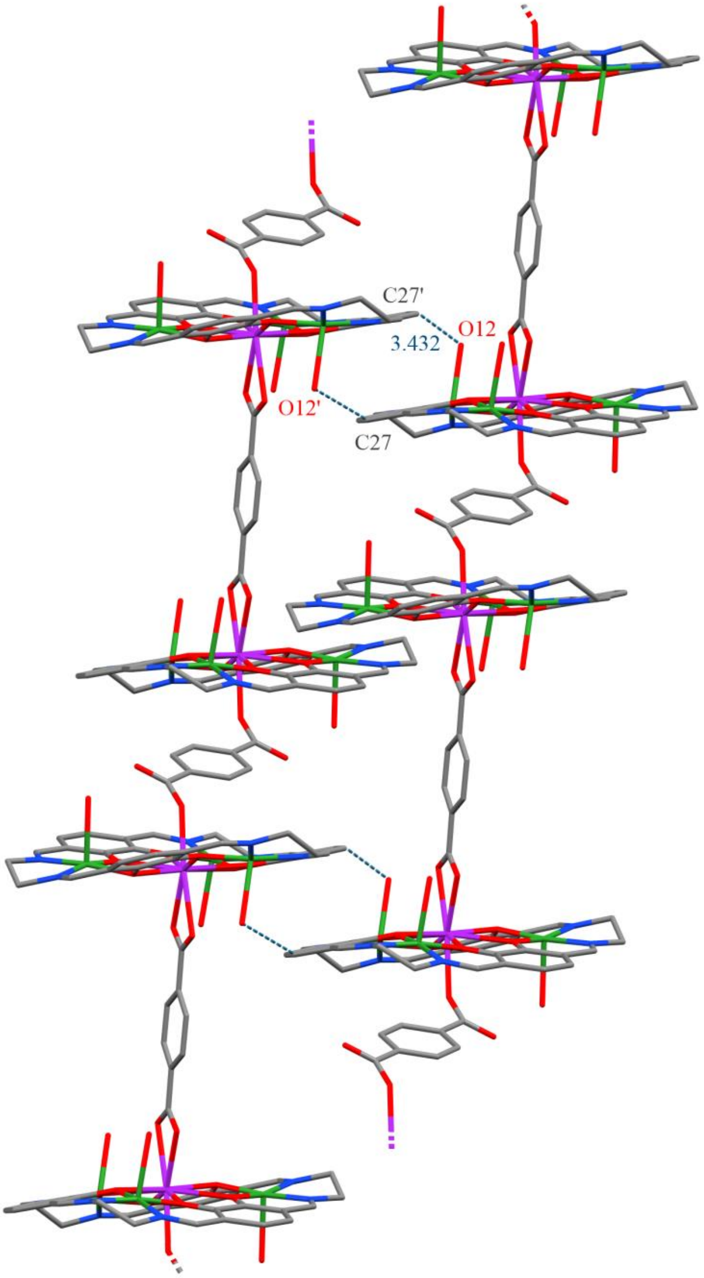

Figure S7. Perspective view of the packing of the one-dimensional coordination polymer $\{[\mathrm{Cu^{II}}_3\mathrm{Tb^{III}}(\mathbf{L}^{\mathbf{Et}})(\mathrm{tpa})(\mathrm{H_2O})_3](\mathrm{NO_3})\cdot0.5\mathrm{H_2O}\cdot0.25\mathrm{MeOH}\}_n$ (**2**) looking approximately down the *b* axis. All hydrogen atoms and non-coordinating solvent molecules omitted for clarity. Tb, Cu, O, N, and C atoms are represented in purple, green, red, blue and grey, respectively. Distance quoted in blue is given in Å.

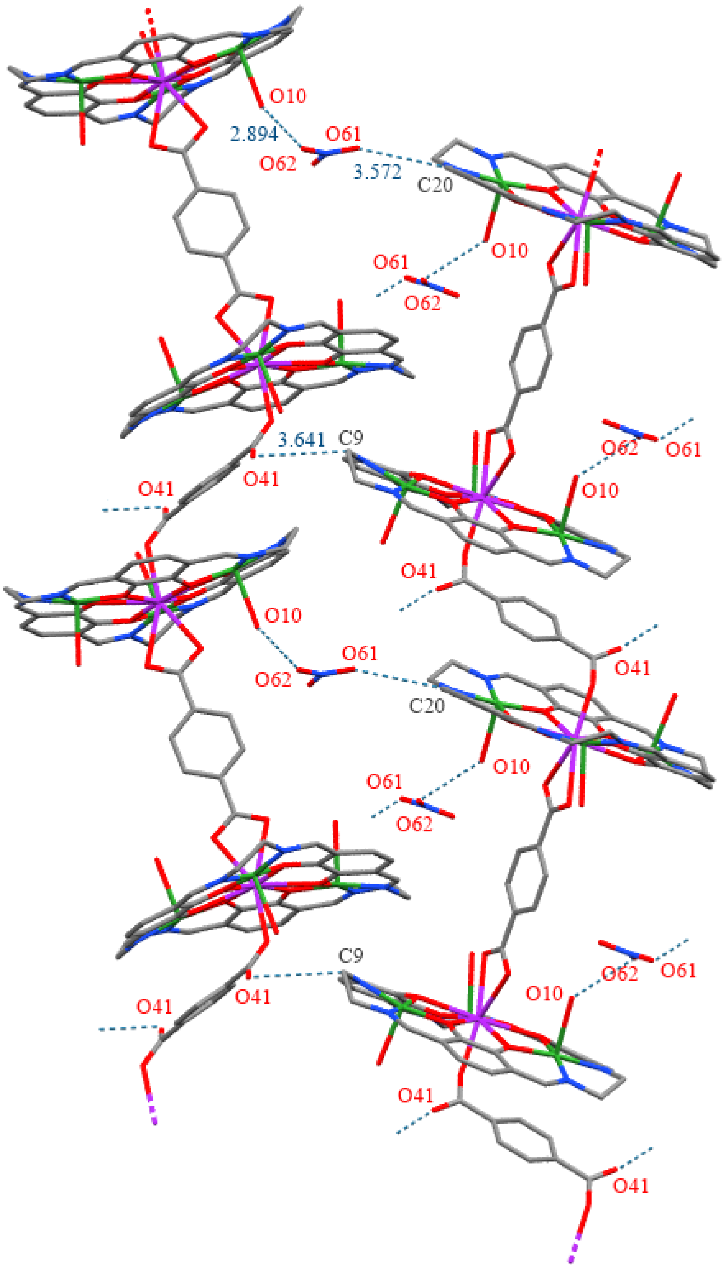

Figure S8. Perspective view of the one-dimensional coordination polymer $\{[\mathrm{Cu^{II}_3Tb^{III}}(\mathbf{L}^{\mathbf{Et}})(\mathrm{tpa})(\mathrm{H_2O})_3](\mathrm{NO_3})\cdot 0.5\mathrm{H_2O}\cdot 0.25\mathrm{MeOH}\}_n$ (**2**) looking down between the *a* and the *c* axis. All hydrogen atoms and non-coordinating solvent molecules omitted for clarity. Tb, Cu, O, N, and C atoms are represented in purple, green, red, blue and grey, respectively. Distances quoted in blue are given in Å.

Table S4. Results of the SHAPE[7] analysis for the Tb^{III} ion for **2**. These idealised nine coordinate geometries are shown in Figure S4. If the value of the SHAPE analysis is 0 then the corresponding structure is fully coincident in shape with the reference polyhedron P, whereas the maximum allowed value of 100 corresponds to the hypothetical case in which all atoms of the molecule occupy the same point in space.

geometry of Tb^{III}	CCU-9[a]	CSAPR-9[a]	TCTPR-9[a]	JTDIC-9[a]	HH-9[a]	MFF-9[a]
in **2**	3.996	10.116	10.478	9.395	**1.282**	8.140

[a] CCU-9: Capped cube, *C4v*; CSAPR-9: Capped square antiprism, *C4v*; TCTPR-9: Tricapped trigonal prism, *D3h*; JTDIC-9 Tridiminished icosahedron (J63), *C3v*; HH-9: Hula-hoop, *C2v*; MFF-9: Muffin, *Cs*.

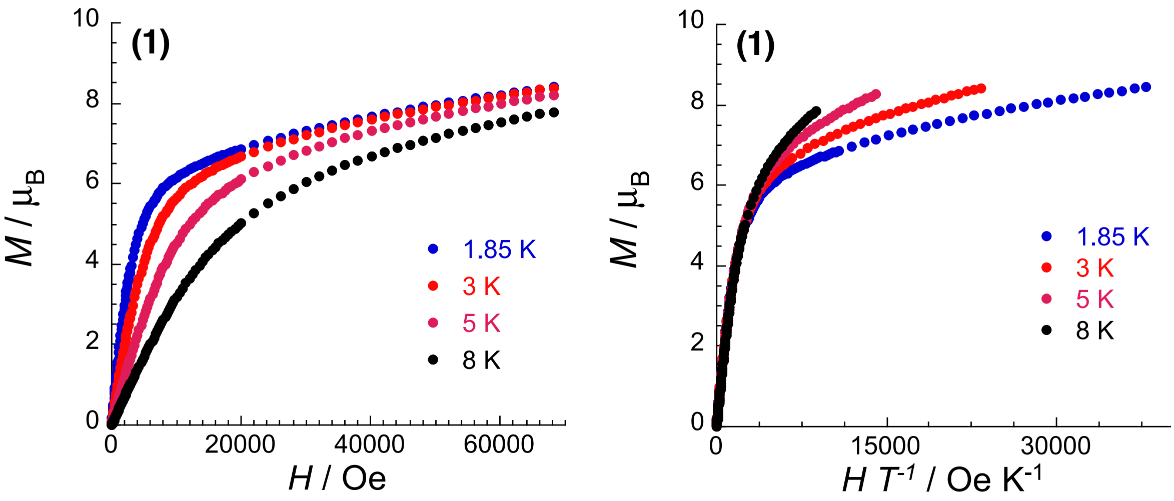

Figure S9. Field dependence of magnetisation for **1** plotted as M versus H (left) or M versus H/T (right) at the temperatures indicated, scanning at 80 – 400 Oe.min^{-1} for $H < 1$ T and 500 – 2500 Oe.min^{-1} for $H > 1$ T.

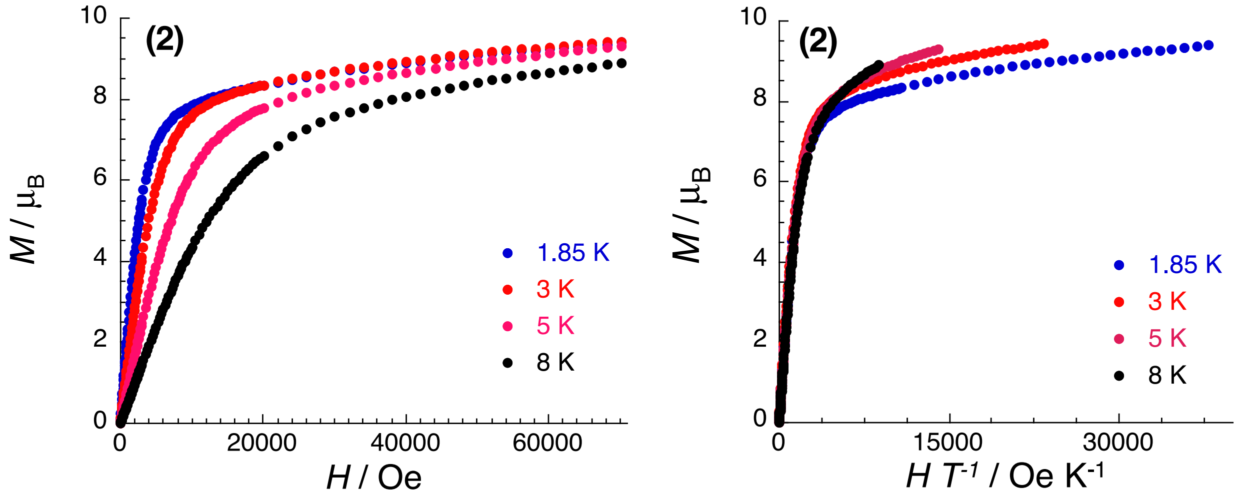

Figure S10. Field dependence of magnetisation for **2** plotted as M versus H (left) or M versus H/T (right) at the temperatures indicated, scanning at 80 – 400 Oe.min^{-1} for $H < 1$ T and 500 – 2500 Oe.min^{-1} for $H > 1$ T.

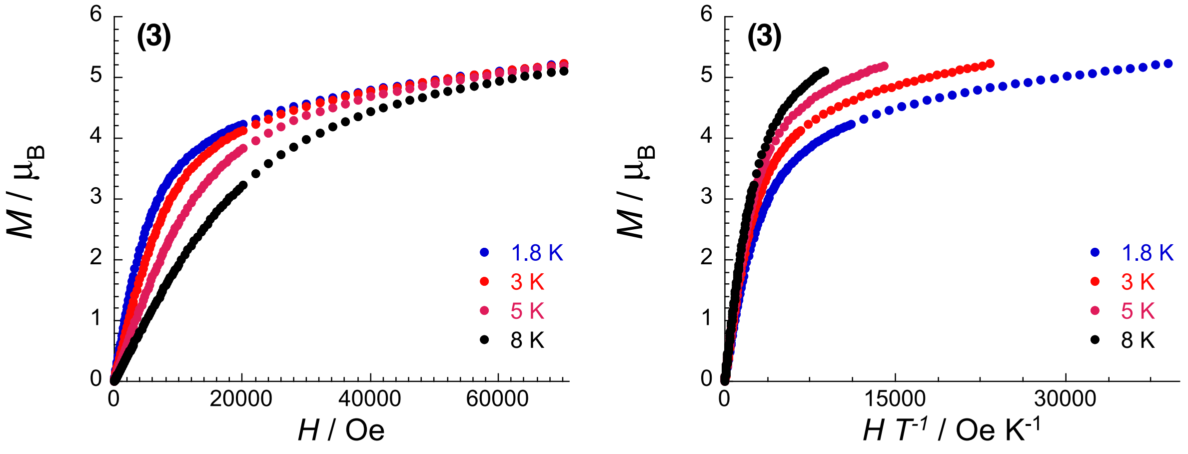

Figure S11. Field dependence of magnetisation for **3** plotted as M versus H (left) or M versus H/T (right) at the temperatures indicated, scanning at 80 – 400 Oe.min^{-1} for $H < 1$ T and 500 – 2500 Oe.min^{-1} for $H > 1$ T.

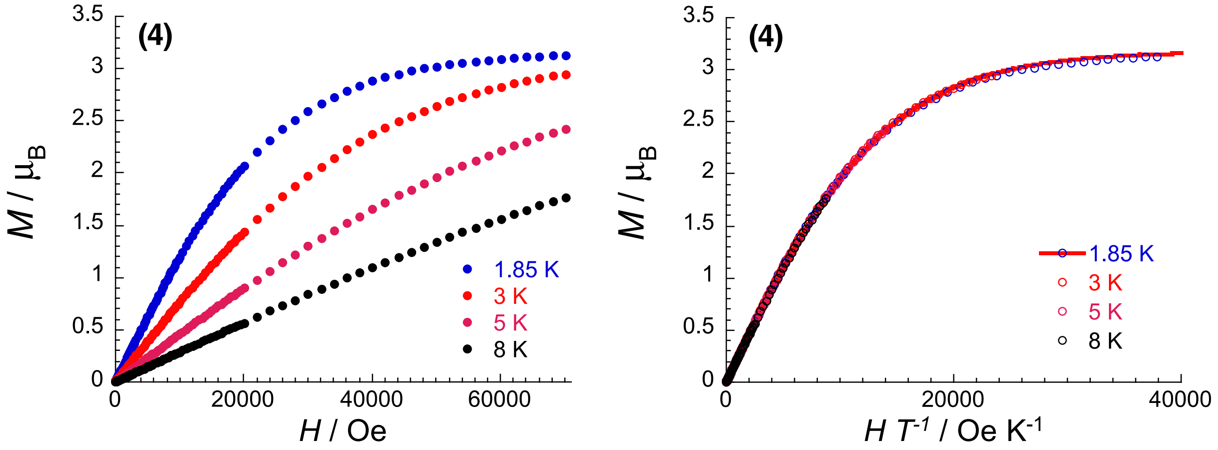

Figure S12. Field dependence of magnetisation for **4** plotted as M versus H (left) or M versus H/T (right) at the temperatures indicated, scanning at 80 – 400 Oe.min^{-1} for $H < 1$ T and 500 – 2500 Oe.min^{-1} for $H > 1$ T. Solid line on M versus H/T plot is the best fit of the experimental data to the sum of three $S = 1/2$ Brillouin functions.

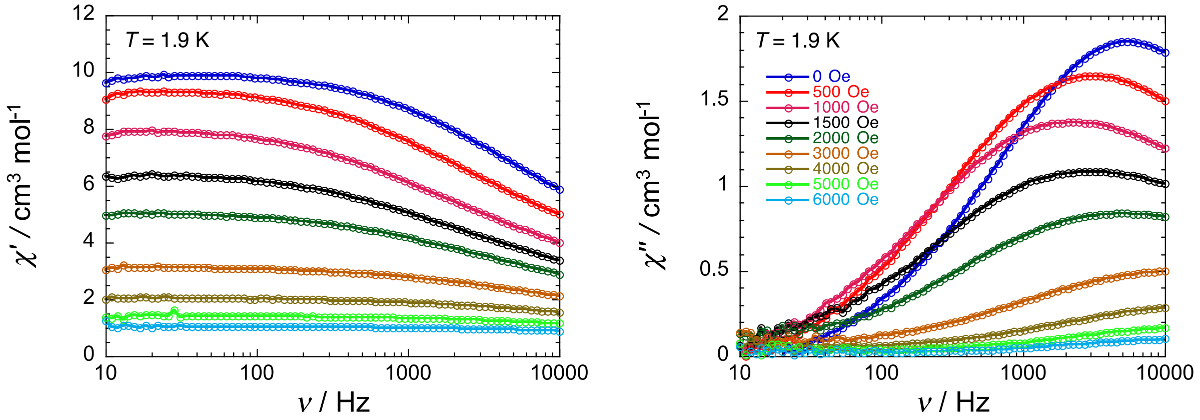

Figure S13. Frequency dependence of the real (χ', left) and imaginary (χ'', right) components of the ac susceptibility, at the dc fields indicated for **1** at 1.9 K. Solid lines are visual guides.

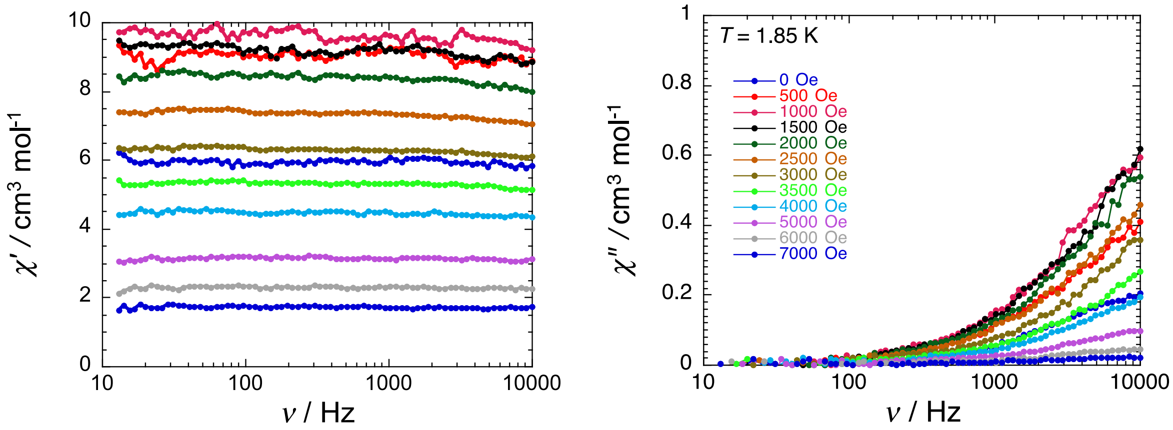

Figure S14. Frequency dependence of the real (χ', left) and imaginary (χ'', right) components of the ac susceptibility, between 0 and 7000 Oe and between 10 and 10000 Hz, for **2** at 1.85 K. Solid lines are visual guides.

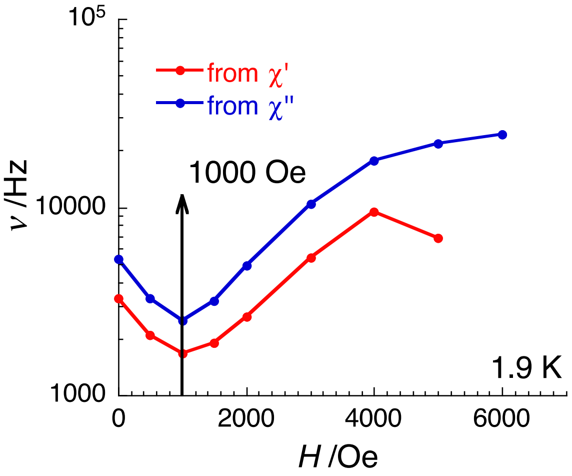

Figure S15. Field dependence of the characteristic relaxation frequency for **1** at 1.9 K extracted from Figure S13 by using a generalized Debye model to fit the real (χ', red dots) and imaginary (χ'', blue dots) components of the ac susceptibility. Solid lines are visual guides.

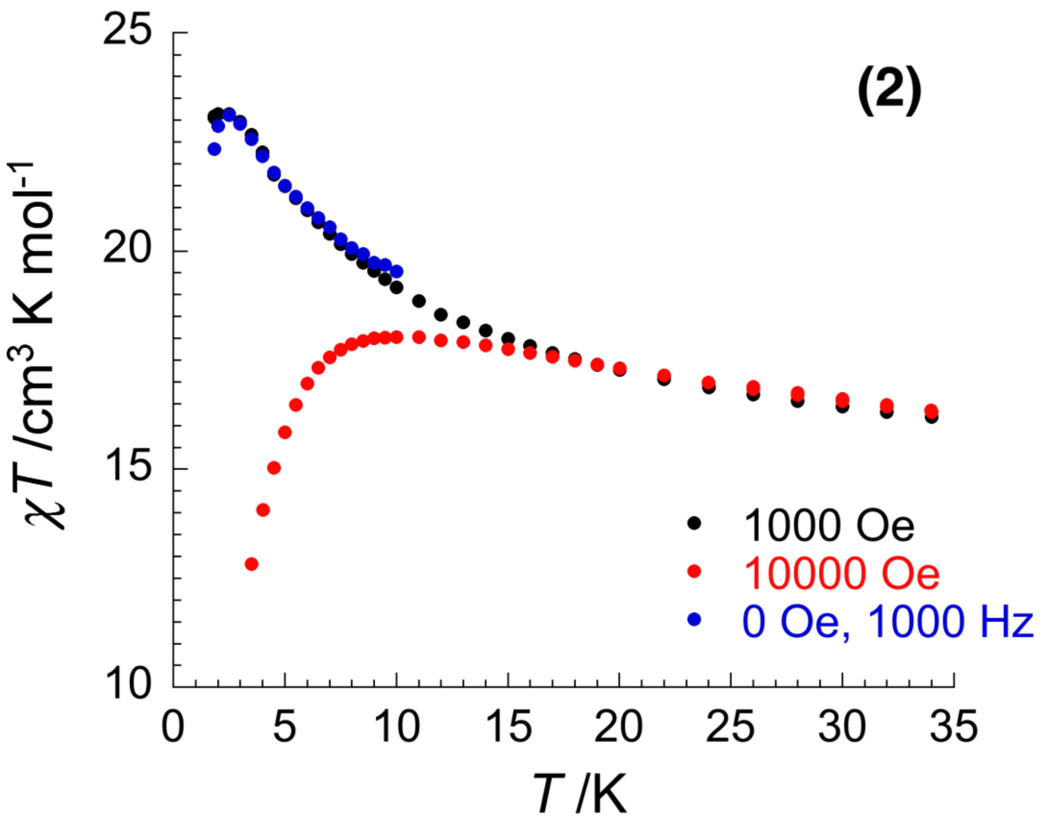

Figure S16. The magnetic behaviour of **2** was first measured in zero-dc field (blue dots), in order to check the absolute susceptibility, even if the ac measurements are less accurate than the dc ones. Then we did two measurements, first at 0.1 T (black dots) and later (after all the M vs H measurements) at 1 T (red dots). The position of the different data (shown here) clearly and unambiguously confirms that the SQUID sample was NOT oriented in the applied magnetic field at any moment of the measurement.

References

1. J. L. Ellingboe and H. H. Runnels, *J. Chem. Eng. Data*, 1966, **11**, 185-187.
2. S. Akine, T. Taniguchi and T. Nabeshima, *J. Am. Chem. Soc.*, 2006, **128**, 15765-15774.
3. CryAlisPRO, Oxford Diffraction, 2011.
4. L. Palatinus and G. Chapuis, *J. Appl. Crystallogr.*, 2007, **40**, 786-790.
5. G. M. Sheldrick, *Acta Crystallogr., Sect. A: Found. Crystallogr.*, 2008, **A64**, 112-122.
6. A. Ruiz-Martinez and S. Alvarez, *Chem. Eur. J.*, 2009, **15**, 7470-7480.
7. D. Casanova, M. Llunell, P. Alemany and S. Alvarez, *Chem. Eur. J.*, 2005, **11**, 1479-1494.
8. A. Ruiz-Martínez, D. Casanova and S. Alvarez, *Chem. Eur. J.*, 2008, **14**, 1291-1303.